

Sampled-Data Primal-Dual Gradient Dynamics in Model Predictive Control [★]

Ryuta Moriyasu ^a, Sho Kawaguchi ^b, Kenji Kashima ^c

^aToyota Central R&D Labs., Inc., Aichi, Japan

^bToyota Industries Corporation, Aichi, Japan

^cGraduate School of Informatics, Kyoto University, Kyoto, 606-8501, Japan

Abstract

Model Predictive Control (MPC) is a versatile approach capable of accommodating diverse control requirements, holding significant promise for a broad spectrum of industrial applications. Noteworthy challenges associated with MPC include the substantial computational burden and the inherent difficulty in ensuring system stability. Recently, a rapid computation technique has been introduced as a potential solution. This method guides the input toward convergence with the optimal control problem solution by employing the primal-dual gradient (PDG) dynamics as a controller. Furthermore, stability assurances grounded in dissipativity theory have been established. However, these assurances are applicable solely to continuous-time feedback systems. As a consequence, when the controller undergoes discretization and is implemented as a sampled-data system, stability cannot be guaranteed. In this paper, we propose a discrete-time dynamical controller, incorporating specific modifications to the PDG approach, and present stability conditions relevant to the resulting sampled-data system. Additionally, we introduce an extension designed to enhance control performance. Numerical examples substantiate that our proposed method not only enhances control effectiveness but also effectively discerns stability degradation resulting from discretization, a nuance often overlooked by conventional methods.

Key words: Model predictive control; Primal-dual gradient; Sampled-data system; Stability; Dissipativity; Fast computation.

1 Introduction

Model predictive control (MPC) stands out as a promising control methodology in the industrial domain, offering optimal control by explicitly addressing various control requirements, including constraints. Its applications are widespread, spanning automotive control [3,16,15], process control [10,11], air conditioning [1,7,4], and beyond. Despite its potential, practical applications of MPC grapple with significant challenges, notably the formidable computational load and the intricate task of ensuring closed-loop stability [20]. Diverse solutions have been proposed to address these challenges. Stability guarantees often rely on methods utilizing terminal costs and constraints, although careful formulation is imperative [5]. Alternatively, approaches grounded in

Lyapunov constraints offer flexibility but may encounter feasibility issues [12]. To mitigate the computational burden, strategies such as the continuation method [17] and control law approximations [18] have been introduced. However, these methods involve approximations or relaxations of conventional MPC, rendering the aforementioned stability guarantees less directly applicable.

This study zeroes in on instant MPC (iMPC) [22] as a well-balanced solution to the aforementioned challenges. iMPC leverages primal-dual gradient dynamics (PDG) [8,6], where the solution to an optimization problem manifests as a fixed point within continuous-time dynamics. The controller, based on PDG, and the dynamics of the controlled plant evolve concurrently. The PDG does not fully resolve the control problem at each instance; however, it ensures satisfaction of the KKT condition of the original optimal control problem at the equilibrium point of the closed-loop system. This methodology facilitates rapid computations by obtaining control inputs through straightforward calculations of variable time evolution using ordinary differential equations.

[★] This paper was not presented at any IFAC meeting. Corresponding author R. Moriyasu.

Email addresses: moriyasu@mosk.tytlabs.co.jp (Ryuta Moriyasu), sho.kawaguchi@mail.toyota-shokki.co.jp (Sho Kawaguchi), kk@i.kyoto-u.ac.jp (Kenji Kashima).

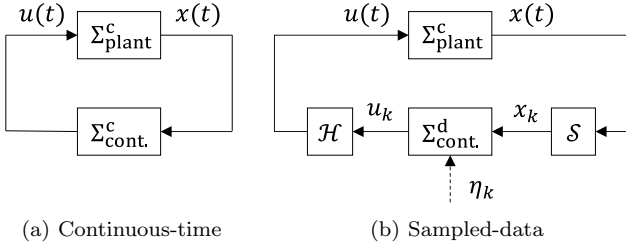


Fig. 1. Schematics of feedback systems. Σ_{plant} , $\Sigma_{\text{cont.}}$, S , \mathcal{H} represent a plant, a controller, a sampler, and a holder, respectively. The superscript c, d indicate continuous-time and discrete-time, respectively.

Moreover, the stability of the closed-loop system can be guaranteed by considering the dynamical controller and the plant's dissipative nature.

Despite its merits, challenges persist regarding stability in implementation and potential performance degradation. The method's stability guarantee pertains to continuous-time (Figure 1(a)), and when discretized for implementation as a sampled-data control system (Figure 1(b)), preservation of stability is not assured, potentially leading to divergence. Additionally, as mentioned earlier, the method gradually converges the input to the optimal point, introducing a tendency for transient performance degradation until the closed-loop system attains equilibrium.

In light of the aforementioned challenges, we endeavor to extend the capabilities of iMPC to address these issues effectively. Our approach involves introducing a controller that corresponds to the discrete-time version of PDG to tackle the optimal control problem. This discrete-time controller is derived through a modified form of the naive discretization of continuous-time PDG using Eulerian forward difference. A notable distinction from the naive discretization lies in the introduction of a step size for the dual variable, denoted as η in Figure 1(b).

A primary contribution of this study is the derivation of stability conditions for the resulting sampled-data feedback system. This is achieved by explicitly considering the impact of discretization and the sampling period, leveraging a newly proposed step size rule. Another contribution involves the proposal of introducing a gain for the controller, aimed at enhancing control performance.

The paper is organized as follows. The structure and stability conditions of iMPC are succinctly summarized in Section 2, where we also discuss the introduction of controller gains, an aspect not covered in the original paper, to afford more flexible control design. In Section 3, we present our discrete-time controller proposal and elucidate the stability conditions of the resulting sampled-data system. Section 4 details numerical experiments conducted under various parameter settings, evaluating

stability measures based on both conventional theory and our proposed methodology. Furthermore, the effectiveness of the proposed controller is demonstrated in an engine system with strong nonlinear characteristics, comparing its performance with that of ordinary MPC. The concluding Section 5 provides a summary of our findings and their implications.

Notation

Let us denote the set of all positive (nonnegative) vectors in \mathbb{R}^n by $\mathbb{R}_{>0}^n$ ($\mathbb{R}_{\geq 0}^n$); the set of all nonnegative integers by $\mathbb{Z}_{\geq 0}$; a set of integers $\{1, \dots, n\} \subset \mathbb{Z}$ by \mathbb{Z}_n ; the identity matrix of appropriate size by I ; the i -th element of a vector v by $(v)_i$; the sub-vector consisting of $(v)_i, i \in J \subset \mathbb{Z}$ by $(v)_J$; a collective vector $[v_1^\top \dots v_n^\top]^\top$ by $[v_1; \dots; v_n]$; Hadamard product by \circ ; Euclidean norm by $\|\cdot\|$; a weighted vector norm $(x^\top P x)^{1/2}$ with positive semi-definite symmetric matrix P by $\|x\|_P$; and the maximum eigenvalue of a symmetric matrix S by $\lambda_{\max}(S)$. We define an operator

$$[a]_b^+ := \begin{cases} a & (b > 0) \\ \max(0, a) & (b = 0) \end{cases}.$$

For vectors $a \in \mathbb{R}^n, b \in \mathbb{R}_{\geq 0}^n$, $[a]_b^+$ imply the vector whose i -th component is $[(a)_i]_{(b)_i}^+$.

2 Preliminaries

The PDG-based MPC controller named instant MPC (iMPC) [22] and the theory of stability guarantee are outlined here, with certain extensions to the original.

2.1 Problem Statement

We consider a continuous-time linear system Σ_{plant}^c :

$$\dot{x} = A_c x + B_c u, \quad (1)$$

where $x \in \mathbb{R}^n, u \in \mathbb{R}^m$ are the state and input, respectively, and A_c, B_c are constant matrices of appropriate dimensions. We assume the plant has QSR-dissipativity [19]:

Assumption 1 (*Assumption for the plant*)
For $S_{\text{plant}}(x) := \frac{1}{2}x^\top x$, there exists $Q = Q^\top, S, R = R^\top$ such that

$$\dot{S}_{\text{plant}} \leq \begin{bmatrix} x \\ u \end{bmatrix}^\top \begin{bmatrix} Q & S \\ S^\top & R \end{bmatrix} \begin{bmatrix} x \\ u \end{bmatrix}$$

holds for any x, u .

Utilizing the discretized model $x_{k+1} = A_h x_k + B_h u_k$, where $A_h = e^{A_c \Delta \tau}$, $B_h = \int_0^{\Delta \tau} e^{A_c(\Delta \tau - t)} B_c dt$ and $\Delta \tau \in \mathbb{R}_{>0}$ is a discrete time step, we can consider a finite-horizon optimal control problem

Problem 2 (*Optimal control problem*)

$$\begin{aligned} & \underset{w}{\text{minimize}} \quad f(w) \\ & \text{s.t.} \quad g(w) \leq 0, h(w; x) = \begin{bmatrix} x_1 - (A_h x_0 + B_h u_0) \\ \vdots \\ x_N - (A_h x_{N-1} + B_h u_{N-1}) \end{bmatrix} = 0, \end{aligned}$$

where f, g, h are the objective function, inequality constraint function, and equality constraint function, respectively, and $w := [x_{1:N}; u_{0:N-1}] \in \mathbb{R}^{(n+m)N}$ is a combined vector consisting of state sequence $x_{1:N} := [x_1; \dots; x_N] \in \mathbb{R}^{nN}$ and input sequence $u_{0:N-1} := [u_0; \dots; u_{N-1}] \in \mathbb{R}^{mN}$ with horizon length $N \in \mathbb{N}$ and initial state $x_0 = x$.

Additionally, $h(w; x)$ can include any linear equality constraint. We assume Problem 2 to exhibit the following properties:

Assumption 3 (*Assumption for the control problem*)

- a) $g(0) \leq 0, \nabla f(0) = 0$.
- b) f is strictly convex, g is convex, and h is affine as $h(w; x) = Cw + Dx$.
- c) There exists $\rho \in \mathbb{R}_{>0}$ satisfying $\nabla f^\top w \geq \rho w^\top w$ for any w .

2.2 Instant MPC

A continuous-time dynamics $\Sigma_{\text{cont.}}^c$:

$$\begin{aligned} \dot{w} &= -\zeta \left(\nabla f(w) + \nabla g(w)\mu + \kappa \nabla h(w; x) \left(\lambda + \frac{\beta}{\zeta} \dot{\lambda} \right) \right), \\ \dot{\mu} &= \zeta [g(w)]_\mu^+, \\ \dot{\lambda} &= \zeta \tau (-\alpha \lambda + h(w; x)), \\ u &= Ew, \end{aligned}$$

called iMPC provides input close to the solution of Problem 2. Here, $\mu \in \mathbb{R}^{n_\mu}, \lambda \in \mathbb{R}^{n_\lambda}$ are the dual variables corresponding to the inequality and equality constraints, respectively, $\alpha \in \mathbb{R}_{>0}, \beta \in \mathbb{R}_{\geq 0}, \zeta \in \mathbb{R}_{>0}$ are scalar constants. E is a constant matrix satisfying $Ew = u_0$, and $\kappa := 1 + 2\alpha\beta, \tau := (1 + \alpha\beta)^{-1}$. The proposed controller can be viewed as a variation of primal-dual gradient (PDG) dynamics [6], incorporating a slight modification to enable adjustable dissipativity. The parameter ζ introduced here is absent in the original study [22]. This constant gain serves as an essential factor for tuning the overall response speed of the controller. Subsequently, in the ensuing propositions, adjustments are made to the

results presented in the original paper to accommodate the inclusion of the parameter ζ into the framework.

Remark 4 Assume that x is fixed at some point, the constant gain ζ can adjust the speed to reach the fixed point of $\Sigma_{\text{cont.}}^c$:

$$\begin{aligned} \nabla f(w) + \nabla g(w)\mu + \kappa \nabla h(w; x)\lambda &= 0, \\ [g(w)]_\mu^+ &= 0, h(w; x) = \alpha\lambda. \end{aligned} \quad (2)$$

This condition does not exactly correspond to the KKT condition of Problem 2:

$$\begin{aligned} \nabla f(w) + \nabla g(w)\mu + \nabla h(w; x)\lambda &= 0, \\ [g(w)]_\mu^+ &= 0, h(w; x) = 0. \end{aligned} \quad (3)$$

This observation implies that even when the input satisfies the equilibrium condition (2) corresponding to x at each time, the resultant trajectory of the feedback system ($\Sigma_{\text{plant}}^c, \Sigma_{\text{cont.}}^c$) may not align with the solution to Problem 2. Nevertheless, in the event that the origin $(w, \mu, \lambda, x) = (0, 0, 0, 0)$ of the feedback system is asymptotically stable, the point corresponding to (2) asymptotically converges to the KKT point (3).

The subsequent results pertain to the stability analysis of the continuous-time feedback system ($\Sigma_{\text{plant}}^c, \Sigma_{\text{cont.}}^c$).

Lemma 5 [22] Let $S_{\text{cont.}}(w, \mu, \lambda) := \frac{1}{2}(w^\top w + \mu^\top \mu + \lambda^\top \lambda)$ be the storage function of $\Sigma_{\text{cont.}}^c$. Under Assumption 3, the dissipation inequality

$$\dot{S}_{\text{cont.}} \leq \zeta \begin{bmatrix} w \\ x \end{bmatrix}^\top \begin{bmatrix} -\rho I - \beta C^\top C & -\beta C^\top D \\ -\beta D^\top C & \frac{\tau}{4\alpha} D^\top D \end{bmatrix} \begin{bmatrix} w \\ x \end{bmatrix},$$

holds for any w, x .

Proposition 6 [22] Under Assumptions 1 and 3, if there exists $\delta \in \mathbb{R}_{>0}$ satisfying

$$\begin{aligned} Q_{\text{wx}} &:= \begin{bmatrix} -\rho I - \beta C^\top C + \delta E^\top R E & -\beta C^\top D + \delta E^\top S^\top \\ -\beta D^\top C + \delta S E & \frac{\tau}{4\alpha} D^\top D + \delta Q \end{bmatrix} \\ &< 0, \end{aligned}$$

then $(w, \lambda, x) = (0, 0, 0)$ is globally asymptotically stable and $(w, \mu, \lambda, x) = (0, 0, 0, 0)$ is Lyapunov stable.

2.3 Additional Considerations

The presented Proposition 6 stands as the central outcome in the literature [22]. Asymptotic stability of the dual variable μ is not claimed in the result. However, it can be feasibly demonstrated by introducing a slight refinement to Assumption 3, as follows:

Assumption 7 (Slightly tightened assumption for the control problem)

- a) $g(0) < 0, \nabla f(0) = 0$.
- b) f is strictly convex, g is convex, and h is affine as $h(w; x) = Cw + Dx$.
- c) There exists $\nabla f^\top w \geq \rho w^\top w$ such that $\rho \in \mathbb{R}_{>0}$ for any w .

The modification to Assumption 3(a) involves eliminating the equality for the inequality function g . This, assumption 3(a) necessitates that $w = 0$ serves as an interior point within the feasible set associated with the inequality constraint $g(w) \leq 0$. The implication of this adjustment is encapsulated in the subsequent result.

Theorem 8 Under Assumption 1 and 7, if there exists δ satisfying $Q_{\text{wx}} \prec 0$, then $(w, \mu, \lambda, x) = (0, 0, 0, 0)$ is globally asymptotically stable.

PROOF. Let $V(w, \mu, \lambda, x) := S_{\text{cont.}}(w, \mu, \lambda) + \delta \zeta S_{\text{plant}}(x) (\geq 0)$ be a Lyapunov function candidate, then

$$\dot{V} = \dot{S}_{\text{cont.}} + \delta \zeta \dot{S}_{\text{plant}} \leq -\zeta \| [w; x] \|_{-Q_{\text{wx}}}^2 \leq 0$$

holds from $Q_{\text{wx}} \prec 0$. The following shows that the equality is satisfied ($\dot{V} = 0$) if and only if $(w, \mu, \lambda, x) = (0, 0, 0, 0)$. When $(w, x) \neq (0, 0)$, the equality fails trivially. When $(w, x) = (0, 0)$, equality fails from

$$\begin{aligned} \dot{V} &= \mu^\top \dot{\mu} + \lambda^\top \dot{\lambda} = \zeta (\mu^\top [g(0)]_\mu^+ - \tau \alpha \lambda^\top \lambda) \\ &\leq -\zeta \tau \alpha \lambda^\top \lambda \leq 0 \end{aligned}$$

when $\lambda \neq 0$. When $(w, \lambda, x) = (0, 0, 0)$ and $\mu \neq 0$, the equality fails from

$$\dot{V} = \zeta \mu^\top [g(0)]_\mu^+ = \zeta \mu^\top g(0) < 0.$$

Therefore, the equality holds only if $(w, \mu, \lambda, x) = (0, 0, 0, 0)$. The sufficient condition $(w, \mu, \lambda, x) = (0, 0, 0, 0) \Rightarrow \dot{V} = 0$ holds trivially. \square

Note that the result of Proposition 6 and Theorem 8 remains independent of the controller gain ζ . This signifies that the stability of the continuous-time feedback system ($\Sigma_{\text{plant}}^c, \Sigma_{\text{cont.}}^c$) remains invariant, irrespective of arbitrary adjustments to the response speed of the controller. While the inclusion of the gain enhances control performance, an increase in the gain could have a substantial impact on stability when the controller is implemented as a sampled-data system. Therefore, we need to quantitatively assess the effect of discretization on stability.

The following lemma clarifies the results of the next section.

Lemma 9 $Q_{\text{wx}} \prec 0$ is equivalent to $Q_{\text{all}} :=$

$$\begin{bmatrix} -\rho I - \tau \kappa \beta C^\top C + \delta E^\top R E & -\frac{\tau \kappa \beta}{2} C^\top D + \delta E^\top S^\top & -\tau \alpha \beta C^\top \\ -\frac{\tau \kappa \beta}{2} D^\top C + \delta S E & \delta Q & \frac{\tau}{2} D^\top \\ -\tau \alpha \beta C & \frac{\tau}{2} D & -\tau \alpha I \end{bmatrix}$$

$\prec 0$.

PROOF. Since $-\tau \alpha I \prec 0$, $Q_{\text{all}} \prec 0$ is equivalent to the condition for the Schur complement

$$\begin{aligned} &\begin{bmatrix} -\rho I - \tau \kappa \beta C^\top C + \delta E^\top R E & -\frac{\tau \kappa \beta}{2} C^\top D + \delta E^\top S^\top \\ -\frac{\tau \kappa \beta}{2} D^\top C + \delta S E & \delta Q \end{bmatrix} \\ &- \begin{bmatrix} -\tau \alpha \beta C^\top \\ \frac{\tau}{2} D^\top \end{bmatrix} (-\tau \alpha I)^{-1} \begin{bmatrix} -\tau \alpha \beta C & \frac{\tau}{2} D \end{bmatrix} \\ &= Q_{\text{wx}} \prec 0. \end{aligned}$$

\square

3 Method

In this section, we introduce a model predictive controller based on discrete-time PDG, ensuring stability while treating the feedback system as a sampled-data system.

3.1 Problem Statement

We examine the sampled-data system, illustrated in Figure 1(b), which comprises a sampler \mathcal{S} with a sampling period $\Delta t \in \mathbb{R}_{>0}$ and a zero-order holder \mathcal{H} . This configuration is described by $x_k = x(k\Delta t)$ and $u(k\Delta t + d) = u_k$ ($0 \leq d < \Delta t, k \in \mathbb{Z}_{\geq 0}$). Subsequently, the cascaded connection of $\mathcal{H}, \Sigma_{\text{plant}}^c, \mathcal{S}$ can be precisely transformed into a discrete-time linear system Σ_{plant}^d :

$$x_{k+1} = A_d x_k + B_d u_k,$$

where $A_d = e^{A_c \Delta t}, B_d = \int_0^{\Delta t} e^{A_c(\Delta t - \tau)} B_c d\tau$. Consequently, ensuring the stability of the sampled-data feedback system is equivalent to ensuring the stability of the discrete-time feedback system ($\Sigma_{\text{plant}}^d, \Sigma_{\text{cont.}}^d$).

We assume that the plant satisfies

Assumption 10 There exist matrices Q, R, S, T, U, V

satisfying

$$x_k^\top \Delta x_k \leq \Delta t \begin{bmatrix} x_k \\ u_k \end{bmatrix}^\top \begin{bmatrix} Q & S \\ S^\top & R \end{bmatrix} \begin{bmatrix} x_k \\ u_k \end{bmatrix},$$

$$\Delta x_k^\top \Delta x_k \leq (\Delta t)^2 \begin{bmatrix} x_k \\ u_k \end{bmatrix}^\top \begin{bmatrix} T & U \\ U^\top & V \end{bmatrix} \begin{bmatrix} x_k \\ u_k \end{bmatrix},$$

where $\Delta x_k := x_{k+1} - x_k = (A_d - I)x_k + B_d u_k$.

Problem 2 for this system is structured in a manner analogous to the previous section. The sampling period Δt of the described system and the time step $\Delta \tau$ in Problem 2 can be distinct. Here, alongside Assumption 7, we introduce an additional consideration:

Assumption 11 *There exists matrices X, Y, Z satisfying*

$$(\nabla f)^\top (\nabla f + 2\tau\kappa\nabla h(\lambda_k + \beta h)) \leq z_k^\top \begin{bmatrix} X & Y & Z \\ Y^\top & O & O \\ Z^\top & O & O \end{bmatrix} z_k,$$

where $z_k := [w_k; x_k; \lambda_k]$.

Remark 12 *Assumption 10 is an extension of Assumption 3, and for a nominal plant Σ_{plant}^d , we consider $Q = (A_d - I)/\Delta t, S = B_d/\Delta t, R = O, T = (A_d - I)^\top (A_d - I)/(\Delta t)^2, U = (A_d - I)^\top B_d/(\Delta t)^2, V = B_d^\top B_d/(\Delta t)^2$. Notably, $A_d - I \rightarrow A_c, B_d \rightarrow B_c$ at $\Delta t \rightarrow 0$. Assumption 11 is an addition to Assumption 7. If we use a quadratic objective $f(w) = \frac{1}{2}\|w\|_P^2$ ($P = P^\top, P \succ 0$), we let $X = P^2 + 2\tau\kappa\beta PC^\top C, Y = \tau\kappa\beta PC^\top D, Z = \tau\kappa PC^\top$.*

3.2 Controller Design

We consider a discrete-time dynamical controller $\Sigma_{\text{cont.}}^d$:

$$w_{k+1} = w_k + \Delta w_k,$$

$$\mu_{k+1} = \mu_k + \Delta \mu_k,$$

$$\lambda_{k+1} = \lambda_k + \Delta \lambda_k,$$

$$\Delta w_k := -\zeta \Delta t \left(\nabla f + \nabla g(\eta_k \circ \mu_k) + \kappa \nabla h \left(\lambda_k + \frac{\beta \Delta \lambda_k}{\zeta \Delta t} \right) \right),$$

$$\Delta \mu_k := \zeta \Delta t \eta_k \circ [g(w_k)]_{\mu_k}^+,$$

$$\Delta \lambda_k := \zeta \tau \Delta t (-\alpha \lambda_k + h(w_k; x_k)),$$

$$u_k = E w_k,$$

where η is a step size vector of the same dimension as μ . If η is set to a fixed unit vector, this controller aligns with a discretization of $\Sigma_{\text{cont.}}^c$ using Eulerian forward

differences. In other words, the primary distinction between the naive implementation of iMPC and our proposed system lies in how the step size η_k (depicted in Figure 1(b)) is determined.

We put forth a step size rule for η aimed at ensuring the non-negativity of μ and the stability of the system.

Definition 13 (*Step size rule*)

$$\eta_k := \gamma_k \circ \bar{\eta}_k,$$

$$\bar{\eta}_k := (\bar{\eta}_k)_i = \begin{cases} 1 & \text{if } (\mu_k)_i + \zeta \Delta t ([g(w_k)]_{\mu_k}^+)_i \geq 0 \\ \frac{-(\mu_k)_i}{\zeta \Delta t ([g(w_k)]_{\mu_k}^+)_i} & \text{(otherwise)} \end{cases}, \quad (4)$$

$$\gamma_k := (\gamma_k)_i = \begin{cases} \gamma_k^n := \min(1, -c^n (\theta_k^n)^\top \bar{\eta}_k^n) & (i \in I_k^n) \\ \gamma_k^p := \min(1, c^p (-b_k + \sqrt{b_k - 4a_k c_k})) & (i \in I_k^p) \end{cases}, \quad (5)$$

$$I_k^n := \{i \in \mathbb{Z}_{n_\mu} \mid (\theta_k)_i < 0\}, I_k^p := \{i \in \mathbb{Z}_{n_\mu} \mid (\theta_k)_i \geq 0\},$$

$$\theta_k := \mu_k \circ \left([g(w_k)]_{\mu_k}^+ - (\nabla g)^\top w_k + \zeta \Delta t (\nabla g)^\top (\nabla f + \tau\kappa \nabla h(\lambda_k + \beta h)) \right), \quad (6)$$

$$\Pi_k := \frac{\zeta \Delta t}{2} \left(\text{diag}([g(w_k)]_{\mu_k}^+)^2 + \|\nabla g\|^2 \text{diag}(\mu_k)^2 \right), \quad (7)$$

$$a_k := \|\bar{\eta}_k^n\|^2 \|\Pi_k\|, \quad b_k := \|\bar{\eta}_k^p\| \|\theta_k^p\|, \quad (8)$$

$$c_k := \gamma_k^n \left(\gamma_k^n \|\bar{\eta}_k^n\|^2 \|\Pi_k\| + (\theta_k^n)^\top \bar{\eta}_k^n \right) + c^q \lambda_{\max}(Q_{\text{all}}^d) \|z_k\|^2, \quad (9)$$

where $\bar{\eta}_k^n := (\bar{\eta}_k)_{I_k^n}, \theta_k^n := (\theta_k)_{I_k^n}, \bar{\eta}_k^p := (\bar{\eta}_k)_{I_k^p}, \theta_k^p := (\theta_k)_{I_k^p}$, and c^n, c^p, c^q are positive constants that satisfy $c^n < 1/(\|\bar{\eta}_k^n\|^2 \|\Pi_k\|), c^p < 1/(2a_k), c^q < 1$, respectively.

The above definition is rather complicated: Initially, (4) establishes the maximum step size $\bar{\eta}$ to ensure the non-negativity of μ in the subsequent step. Thereafter, actual step size η is obtained by multiplying coefficient (5) with (4). The coefficient (5) is determined within the range $[0, 1]$, considering stability measures (6)-(9). Since the coefficients tend to be 1 for numerous cases, minimal disparity in control performance is noted. The variables dependent on the index sets I_k^n, I_k^p should be treated as 0 if each set is empty.

Next, we examine the stability of the closed-loop system $(\Sigma_{\text{plant}}^d, \Sigma_{\text{cont.}}^d)$, utilizing an assumption

Assumption 14 *There exists $\delta \in \mathbb{R}_{>0}$ that satisfies $Q_{\text{all}}^d := Q_{\text{all}} + Q_{\text{plant}}^d + Q_{\text{cont.}}^d \prec 0$, where*

$$Q_{\text{plant}}^d := \frac{1}{2} \delta \Delta t \begin{bmatrix} E^\top V E & E^\top U^\top & O \\ U E & T & O \\ O & O & O \end{bmatrix},$$

$$Q_{\text{cont.}}^{\text{d}} := \frac{1}{2} \zeta \Delta t \begin{bmatrix} C^{\top} F C + X & C^{\top} F D + Y & C^{\top} G + Z \\ D^{\top} F C + Y^{\top} & D^{\top} F D & D^{\top} G \\ G C + Z^{\top} & G D & H \end{bmatrix},$$

$$F := \tau^2 (I + \kappa^2 \beta^2 C C^{\top}), G := \tau^2 (-\alpha I + \kappa^2 \beta C C^{\top}),$$

$$H := \tau^2 (\alpha^2 I + \kappa^2 C C^{\top}).$$

Note that $Q_{\text{plant}}^{\text{d}} \succeq 0, Q_{\text{cont.}}^{\text{d}} \succeq 0$. This assumption is the stability condition corresponding to the condition $Q_{\text{wx}} \prec 0$ in Proposition 6. Considering Lemma 9 ($Q_{\text{wx}} \prec 0 \Leftrightarrow Q_{\text{all}} \prec 0$), $Q_{\text{plant}}^{\text{d}}, Q_{\text{cont.}}^{\text{d}}$ can be considered to indicate the degradation of stability due to the sampled-data implementation.

Remark 15 *An increase in ζ to enhance control performance necessitates a decrease in Δt to meet the aforementioned assumption. As Δt becomes sufficiently small, the effect of $Q_{\text{plant}}^{\text{d}}$ diminishes, i.e., $Q_{\text{all}}^{\text{d}} \approx Q_{\text{all}} + Q_{\text{cont.}}^{\text{d}}$. In such cases, if $\zeta \Delta t$ remains constant, the stability is largely unaffected.*

The following are the main resultant theorems. Proofs are stated in the Appendix. First, we show the equilibrium condition of the controller.

Theorem 16 *Under Assumptions 7,14 and $\mu_0 \geq 0$, the equilibrium condition of $\Sigma_{\text{cont.}}^{\text{d}}$ for some fixed x is*

$$\begin{aligned} \nabla f + \nabla g(\eta_k \circ \mu_k) + \kappa \nabla h \lambda_k &= 0, \\ [g(w_k)]_{\mu_k}^+ &= 0, h(w_k; x_k) = -\alpha \lambda_k. \end{aligned} \quad (10)$$

This condition corresponds to (2) and converges to the KKT condition (3) when $(w, \mu, \lambda, x) \rightarrow (0, 0, 0, 0)$. The crucial aspect is that this condition does not involve $\eta_k \circ [g(w_k)]_{\mu_k}^+ = 0$ but rather $[g(w_k)]_{\mu_k}^+ = 0$. This implies that the equilibrium of the controller must inherently satisfy the inequality condition $g(w) \leq 0$.

The next one states the stability.

Theorem 17 *Under Assumptions 7,10,11,14 and $\mu_0 \geq 0$, the origin $(w, \mu, \lambda, x) = (0, 0, 0, 0)$ of the discrete-time feedback system $(\Sigma_{\text{plant}}^{\text{d}}, \Sigma_{\text{cont.}}^{\text{d}})$ is globally asymptotically stable.*

This theorem establishes the global asymptotic stability of the sampled-data feedback system depicted in Figure 1(b). In proving this theorem, we relied on Assumption 7. Based on Assumption 3, the asymptotic stability of $(w, \lambda, x) = (0, 0, 0)$ can be demonstrated.

4 Numerical Experiments

4.1 Toy Example

In this section, we present a numerical example referring to the literature [22]. The target plant $\Sigma_{\text{plant}}^{\text{c}}$ has one-input, two-state with matrices:

$$A_c = \begin{bmatrix} -4 & -0.03 \\ 0.75 & -10 \end{bmatrix}, B_c = \begin{bmatrix} 2 \\ 0 \end{bmatrix}.$$

We configure a sampled-data feedback system (Figure 1(b)) incorporating the plant described earlier and a discrete-time PDG controller $\Sigma_{\text{cont.}}^{\text{d}}$ with various parameter settings. The objective is to examine the influence of the introduced gain ζ and the sampling period Δt on control performance. Other controller parameters are fixed at $\alpha = 1, \beta = 1.5, c^{\text{n}} = 0.9999 / (\|\bar{\eta}_k^{\text{n}}\|^2 \|\Pi_k\|), c^{\text{p}} = 0.9999 / (2a_k), c^{\text{q}} = 0.9999$. In Problem 2, the control model is derived using $A_h = e^{A_c \Delta \tau}, B_h = \int_0^{\Delta \tau} e^{A_c(\Delta \tau - \tau)} B_c d\tau$ with the time-step $\Delta \tau = 0.1$ s. A target $r = [200/3; 5]$ for the state x and an upper bound $\bar{u} = 160$ for the input u are considered, with the objective function $f(w) = \|w\|_P^2$, where $P = \text{blockdiag}(I_{2N}, I_N/10)$ and the horizon length $N = 30$. The objective function is defined with the error system configured, such that the state and input are zero at the steady state of $x = r$. In other words, when the optimal solution is $w = 0$, the system is in equilibrium at $x = r$.

The case settings and the evaluated stability measures are summarized in Table 1. The case numbers correspond to the controller gain ζ , with larger case numbers indicating higher gains. In the table, $\delta^*, \delta^{\text{d}*}$ are the optimal δ values that minimize the maximum eigenvalue of Q_{all} and $Q_{\text{all}}^{\text{d}}$, obtained using an LMI solver. The resulting minimum of the maximum eigenvalue is also presented as $\lambda_{\text{max}}^*(Q_{\text{all}}), \lambda_{\text{max}}^*(Q_{\text{all}}^{\text{d}})$.

The simulation results corresponding to Cases 1 to 5 are presented in Figures 2 to 6. In each figure, the dashed line represents the reference for the state or the upper

Table 1
Case settings and evaluated stability measures

Case	1	2	3	4	5
Δt	1 ms				0.1 ms
ζ	1	10	100	1000	1000
δ^*	0.3225				
$\lambda_{\text{max}}^*(Q_{\text{all}})$	-0.0549				
$\delta^{\text{d}*}$	0.3490	0.3515	0.4402	43.490	0.4402
$\lambda_{\text{max}}^*(Q_{\text{all}}^{\text{d}})$	-0.0435	-0.0419	-0.0012	34.999	-0.0012

Solid: Result, Dotted: True optimal, Dashed: Reference/Bound

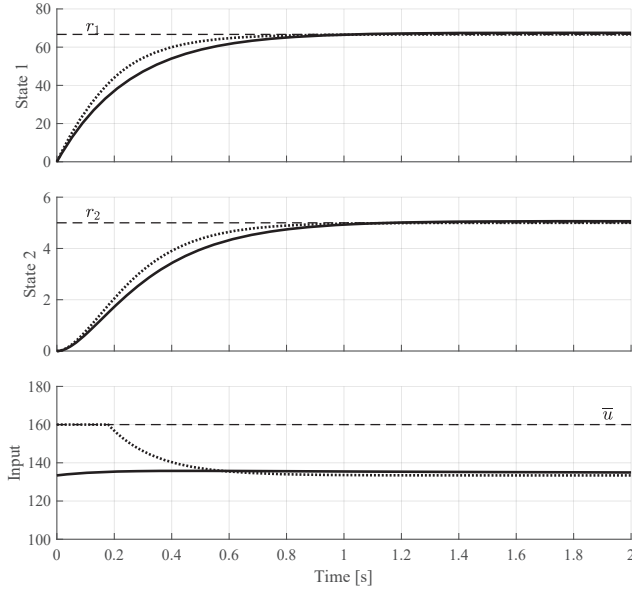


Fig. 2. Results of Case 1 ($\zeta = 1, \Delta t = 1$ ms)

Solid: Result, Dotted: True optimal, Dashed: Reference/Bound

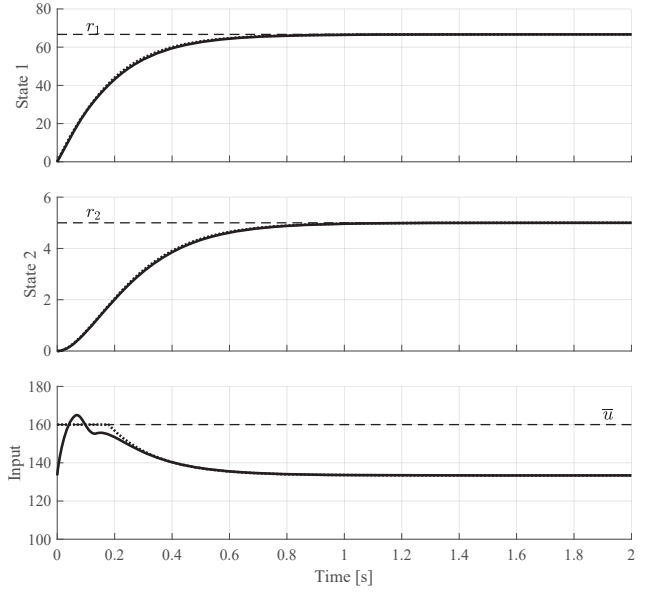


Fig. 4. Results of Case 3 ($\zeta = 100, \Delta t = 1$ ms)

Solid: Result, Dotted: True optimal, Dashed: Reference/Bound

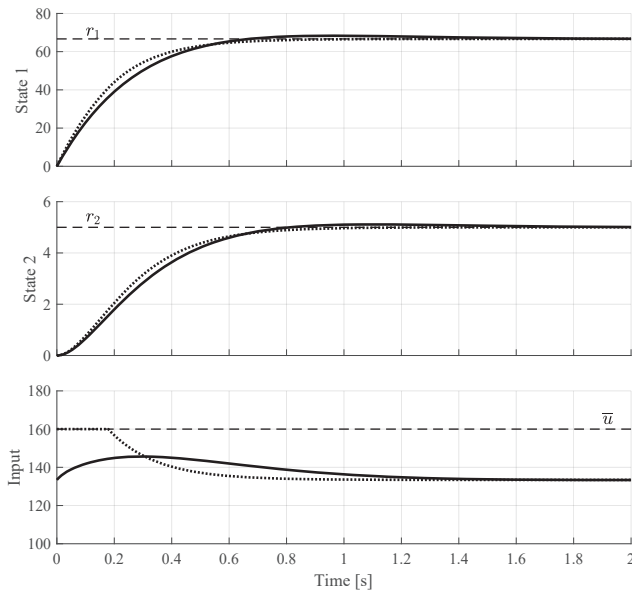


Fig. 3. Results of Case 2 ($\zeta = 10, \Delta t = 1$ ms)

Solid: Result, Dotted: True optimal, Dashed: Reference/Bound

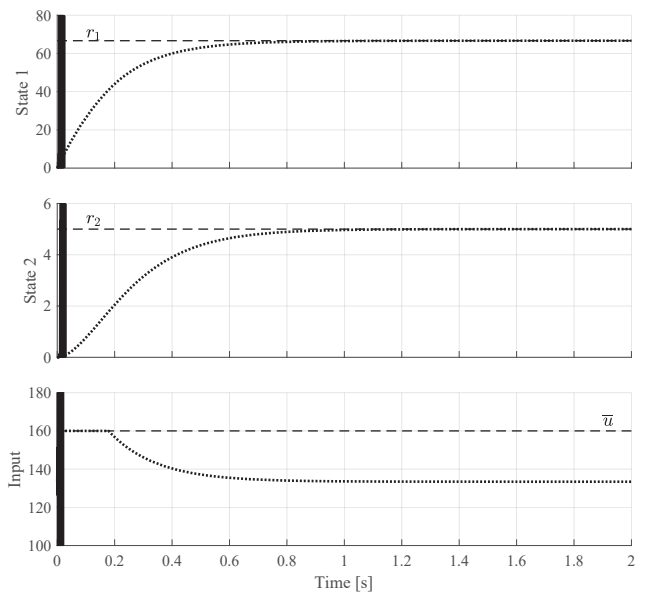


Fig. 5. Results of Case 4 ($\zeta = 1000, \Delta t = 1$ ms)

bound for the input, and the solid line illustrates the control result for each case. As a baseline, the true optimal trajectory, determined by directly solving Problem 2 in each time step, is depicted as dotted lines.

In iMPC theory, the stability of the continuous-time feedback system ($\Sigma_{\text{plant}}^c, \Sigma_{\text{cont.}}^c$) is guaranteed if $\lambda_{\max}^*(Q_{\text{all}})$ is negative. Consequently, the system is deemed stable in all cases due to $\lambda_{\max}^*(Q_{\text{all}}) = -0.0549 < 0$, which is independent of ζ and Δt . In-

deed, the results in Figures 2 to 4 demonstrate stability and improved performance with an increase in the gain ζ . However, as the simulations are conducted through sampled-data implementation, actual stability is compromised, leading to divergence in Case 4 (Figure 5).

In contrast, the proposed method allows for the evaluation of the impact of $\zeta, \Delta t$ on the stability of the sampled-data system through the negative definiteness of Q_{all}^d . Specifically, $\lambda_{\max}^*(Q_{\text{all}}^d)$ is negative in Cases 1-3

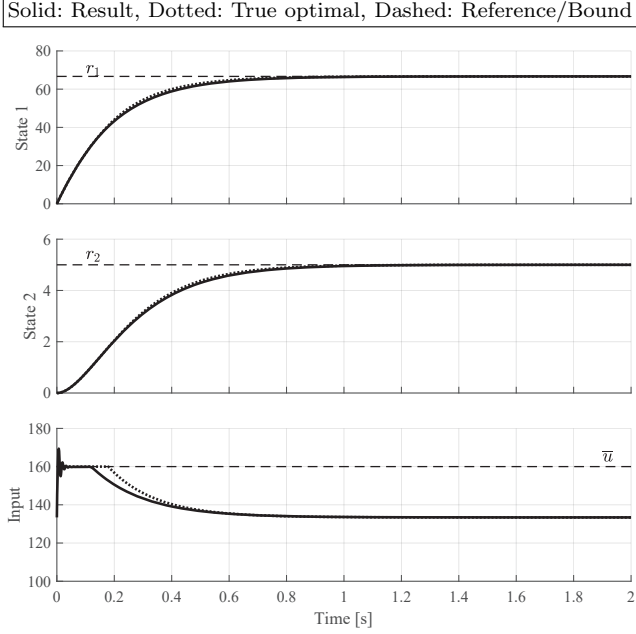


Fig. 6. Results of Case 5 ($\zeta = 1000$, $\Delta t = 0.1$ ms)

but positive in Case 4, indicating potential instability in the latter. Consequently, in Case 5, $\lambda_{\max}^*(Q_{\text{all}}^d)$ is designed to be negative by reducing Δt . Notably, δ^{d*} and $\lambda_{\max}^*(Q_{\text{all}}^d)$ in Case 5 coincide with those in Case 3. This is because $\zeta \Delta t$ exhibits the same value in both cases (see Remark 15). The control result of Case 5 is displayed in Figure 6, confirming that stability is ensured and performance is improved by increasing the gain ζ .

These results support the effectiveness of the proposed method in achieving performance improvement and stability guarantees while accounting for the system being implemented as a sampled-data system. Nevertheless, even with a significantly increased controller gain, the constraint is temporarily violated in certain cases. Therefore, additional countermeasures such as clipping or filtering of the input obtained from the controller are necessary to ensure more stringent constraint fulfillment.

4.2 Engine Air Path System

The proposed method is primarily designed for linear systems; nonetheless, its applicability extends to nonlinear systems through integration with suitable modeling techniques that transform nonlinear systems into an equivalent form amenable to linear analysis [9,13,21,14]. To illustrate this, an application to an engine air path system (Figure 7), recognized for its pronounced nonlinearity, is presented here.

The plant is modeled in a data-driven manner by the structured Hammerstein-Wiener model [13] and is ex-

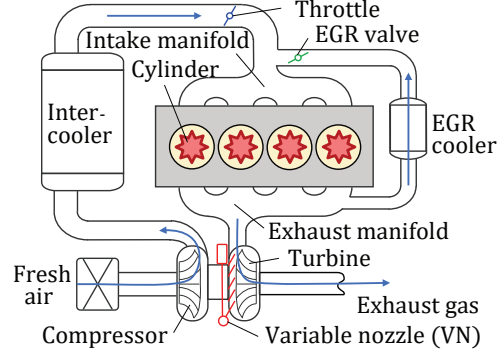


Fig. 7. Engine air path system

pressed as follows:

$$u = \Psi(v), \dot{x} = A_c x + B_c u, y = \Phi^{-1}(x),$$

where Ψ, Φ are homeomorphic maps for v, x , respectively, and Ψ is an element-wise function. The control inputs, denoted as $v = [v_1; v_2; v_3]$, represent the variable turbine nozzle closure, exhaust gas recirculation (EGR) valve opening, and throttle closing, respectively, all expressed in percentage. The upper limit for these inputs is specified as $\bar{v} = [100; 100; 100]$, while the lower limit is set to $\underline{v} = [0; 0; 0]$. The system output, denoted as $y = [y_1; y_2; y_3]$, comprises boost pressure (gas pressure at intake manifold), EGR rate, and pumping mean effective pressure (PMEP) in this order. The corresponding units are kPa, %, and kPa, respectively.

To apply the proposed method to the plant, several variable transformations are necessary. First, the reference for y is converted to the reference for x using Φ . Second, input bounds \bar{v} and \underline{v} are transformed into upper and lower bounds for the internal input u using Ψ . The transformed feasible set for u becomes convex due to the element-wise property of Ψ . Through this procedure, the control problem for y and v is transformed into a problem for x and u , allowing the application of the proposed method.

The controller is configured with the settings $f(w) = 1/2\|w\|$, $\alpha = 1$, $\beta = 1.5$, $c^n = 0.9999/(\|\bar{\eta}_k^n\|^2 \|\Pi_k\|)$, $c^p = 0.9999/(2a_k)$, $c^q = 0.9999$, $N = 10$, $\Delta\tau = 0.1$ s, and the simulation results are shown in Figures 8, 9 and 10, where ζ and Δt are varied within a range ensuring stability. The specific settings are $(\zeta, \Delta t) = (0.5, 10 \text{ ms})$, $(5, 1 \text{ ms})$, and $(50, 0.1 \text{ ms})$, respectively.

In the figures, the dashed lines represent the target values for y and x , as well as the upper and lower bounds for u and v . The solid lines depict the control results obtained with the proposed method, while the dotted lines represent the baseline (the true optimal trajectory).

In each case, the response of the proposed method is slightly slower than the baseline but generally follows

Solid: Result, Dotted: True optimal, Dashed: Reference/Bounds

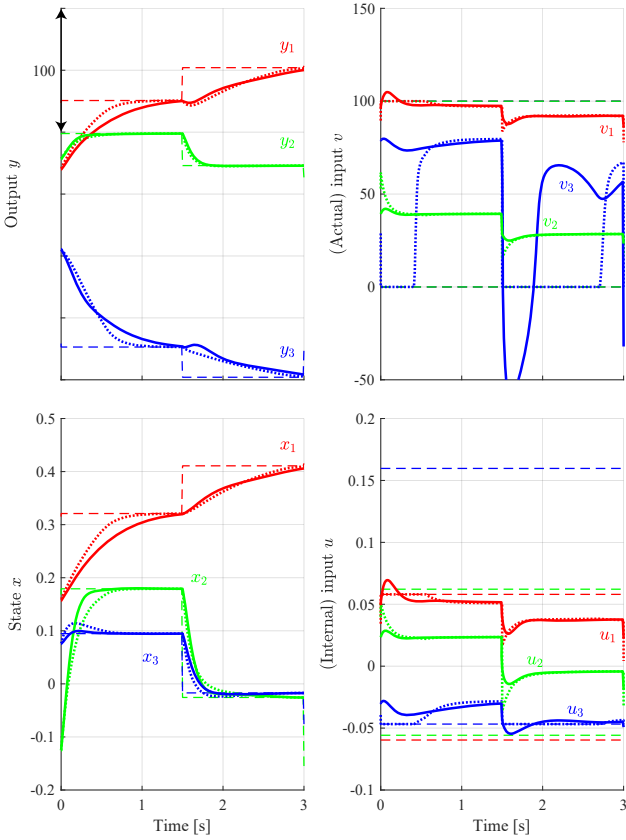


Fig. 8. Simulation results with $\zeta = 0.5, \Delta t = 10$ ms

the reference adequately. For small ζ , constraint fulfillment is slow; however, by increasing ζ , the controller can rapidly bring the inputs within the constraint range. This behavior is attributed to the equilibrium condition of the controller satisfying the inequality constraint (refer to Theorem 16), and an increase in ζ expedites reaching the desired point. Furthermore, the enhancement of tracking performance to the reference by increasing ζ appears relatively modest. This observation may be attributed to the influence of the parameters α and β , introduced to improve stability but potentially reducing the optimality of transients, as evident in (10). This property mirrors the continuous-time case (2), emphasizing the need to reduce conservatism in stability analysis for improved reference tracking while ensuring stability.

The average computation time was 0.048 ms per step (Intel Core i7-1265U, mex execution). Comparatively, the time required to solve the same problem using C/GMRES [17] is 0.40 ms, and that using neural network-based approximation of MPC is 0.073 ms [15]. This indicates that the proposed method achieves speedy computation.

Solid: Result, Dotted: True optimal, Dashed: Reference/Bounds

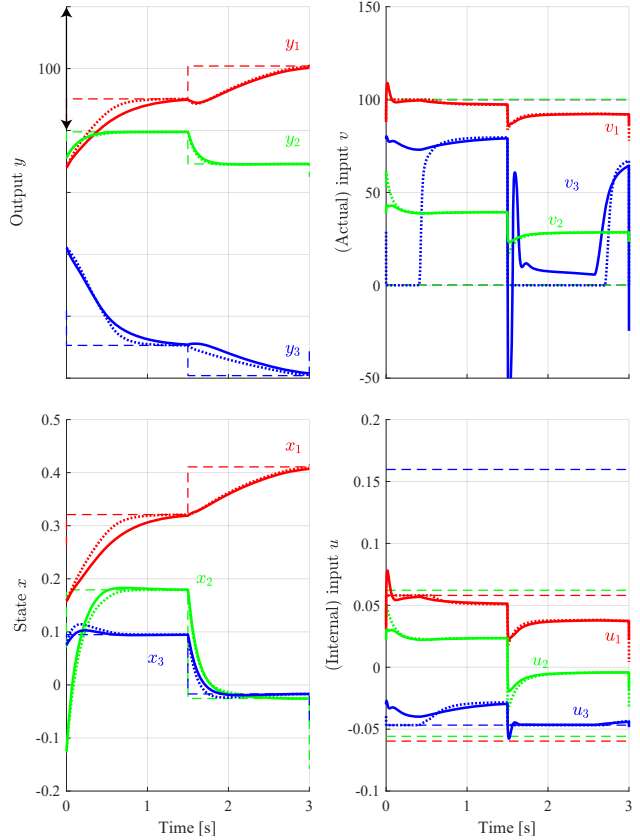


Fig. 9. Simulation results with $\zeta = 5, \Delta t = 1$ ms

5 Conclusion

In summary, we proposed the application of discrete-time primal-dual gradient dynamics to address MPC problems and derived a sufficient condition for ensuring the stability of the resulting sampled-data feedback system. The effectiveness of our stability evaluation method was validated through simple numerical examples, demonstrating its superiority compared with conventional methods. Furthermore, our proposed method exhibited significantly faster computation times in practical examples when compared with other established approaches.

One limitation of our proposed method is that strict constraint fulfillment is not inherently guaranteed. To address this, it would be necessary to design a control system incorporating filter functions, such as control barrier functions [2], when stringent constraint adherence is required. Additionally, since stability assurance heavily depends on the dissipative nature of the plant, it may be challenging or even impossible to guarantee stability for certain types of plants. Future work will focus on resolving these issues and extending the theory and control system to enhance its universality and applicability across a wider range of scenarios.

Solid: Result, Dotted: True optimal, Dashed: Reference/Bounds

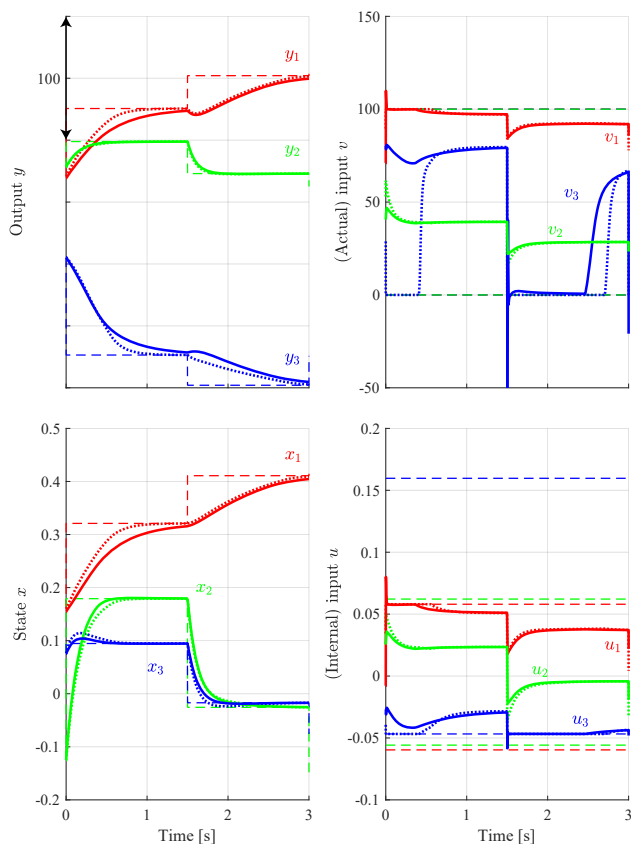


Fig. 10. Simulation results with $\zeta = 50$, $\Delta t = 0.1$ ms

References

- [1] Abdul Afram and Farrokh Janabi-Sharifi. Theory and applications of HVAC control systems—a review of model predictive control (MPC). *Building and Environment*, 72:343–355, 2014.
- [2] Aaron D. Ames, Samuel Coogan, Magnus Egerstedt, Gennaro Notomista, Koushil Sreenath, and Paulo Tabuada. Control Barrier Functions: Theory and Applications. *2019 18th European Control Conference (ECC)*, pages 3420–3431, jun 2019.
- [3] Alberto Bemporad, Daniele Bernardini, Ruixing Long, and Julian Verdejo. Model predictive control of turbocharged gasoline engines for mass production. Technical report, SAE Technical Paper, 2018.
- [4] Felix Bünning, Adrian Schalbetter, Ahmed Aboudonia, Mathias Hudoba de Bady, Philipp Heer, and John Lygeros. Input convex neural networks for building MPC. *arXiv: 2011.13227*, 2020.
- [5] H. Chen and F. Allgöwer. *Nonlinear Model Predictive Control Schemes with Guaranteed Stability*, pages 465–494. Springer Netherlands, Dordrecht, 1998.
- [6] Ashish Cherukuri, Enrique Mallada, and Jorge Cortés. Asymptotic convergence of constrained primal–dual dynamics. *Systems & Control Letters*, 87:10–15, 2016.
- [7] Ján Drgona, Damien Picard, Michal Kvasnica, and Lieve Helsen. Approximate model predictive building control via

machine learning. *Applied Energy*, 218(March):199–216, 2018.

- [8] Diego Feijer and Fernando Paganini. Stability of primal–dual gradient dynamics and applications to network optimization. *Automatica*, 46(12):1974–1981, 2010.
- [9] Milan Korda and Igor Mezić. Linear predictors for nonlinear dynamical systems: Koopman operator meets model predictive control. *Automatica*, 93:149–160, jul 2018.
- [10] A Senthil Kumar and Zainal Ahmad. Model predictive control (MPC) and its current issues in chemical engineering. *Chemical Engineering Communications*, 199(4):472–511, 2012.
- [11] Federico Lozano Santamaria and Jorge M Gómez. An algorithm for tuning NMPC controllers with application to chemical processes. *Industrial & Engineering Chemistry Research*, 55(34):9215–9228, 2016.
- [12] Prashant Mhaskar, Nael H El-Farra, and Panagiotis D Christofides. Stabilization of nonlinear systems with state and control constraints using lyapunov-based predictive control. *Systems & Control Letters*, 55(8):650–659, 2006.
- [13] Ryuta Moriyasu, Taro Ikeda, Sho Kawaguchi, and Kenji Kashima. Structured Hammerstein-Wiener Model Learning for Model Predictive Control. *IEEE Control Systems Letters*, 6:397–402, 2022.
- [14] Ryuta Moriyasu, Masayuki Kusunoki, and Kenji Kashima. Learning exactly linearizable deep dynamics models. In *arXiv*, 2023.
- [15] Ryuta Moriyasu, Sayaka Nojiri, Akio Matsunaga, Toshihiro Nakamura, and Tomohiko Jimbo. Diesel engine air path control based on neural approximation of nonlinear MPC. *Control Engineering Practice*, 91(April):104114, 2019.
- [16] Hayato Nakada, Peter Martin, Anuradha Wijesinghe, Hayato Shirai, Akio Matsunaga, and Hiroyuki Tominaga. An application of C/GMRES model predictive control to a diesel engine air path system. *IFAC-PapersOnLine*, 51(31):529–534, 2018.
- [17] Toshiyuki Ohtsuka. A continuation/GMRES method for fast computation of nonlinear receding horizon control. *Automatica*, 40(4):563–574, apr 2004.
- [18] Thomas Parisini and Riccardo Zoppoli. A receding-horizon regulator for nonlinear systems and a neural approximation. *Automatica*, 31(10):1443–1451, 1995.
- [19] Arash Rahnama, Meng Xia, and Panos J. Antsaklis. A QSR-dissipativity and passivity based analysis of event-triggered networked control systems. In *2016 IEEE 55th Conference on Decision and Control (CDC)*, pages 3072–3077, 2016.
- [20] Sasa V Rakovic and William S Levine. Handbook of model predictive control. 2018.
- [21] Spencer M. Richards, Jean-Jacques Slotine, Navid Azizan, and Marco Pavone. Learning control-oriented dynamical structure from data. In *Proceedings of the 40th International Conference on Machine Learning*, volume 202 of *Proceedings of Machine Learning Research*, pages 29051–29062. PMLR, 2023.
- [22] Keisuke Yoshida, Masaki Inoue, and Takeshi Hatanaka. Instant MPC for Linear Systems and Dissipativity-Based Stability Analysis. *IEEE Control Systems Letters*, 3(4):811–816, 2019.

A Proofs of Main Results

A.1 Properties of Step Size Rule

Lemma 18 *Under Assumption 14 and $\mu_0 \geq 0$, the following claim holds for any $k \in \mathbb{Z}_{\geq 0}$.*

- a) $\mu_k \geq 0$.
- b) $0 \leq \gamma_k^n \leq 1, 0 \leq \gamma_k^p \leq 1, 0 < \bar{\eta}_k \leq 1, 0 \leq \eta_k \leq 1$.
- c) $a_k(\gamma_k^p)^2 + b_k\gamma_k^p + c_k \leq 0$, equality hold iff $c_k = 0$.
- d) $I_k^n \neq \emptyset \Rightarrow 0 < \gamma_k^n \leq 1, 0 < (\eta_k)_{I_k^n} =: \eta_k^n \leq 1, c_k < 0$.
- e) $a_k > 0, c_k < 0 \Rightarrow 0 < \gamma_k^p \leq 1, 0 < (\eta_k)_{I_k^p} =: \eta_k^p \leq 1$.

PROOF.

Proof of (a): We show $\mu_k \geq 0 \Rightarrow \mu_{k+1} \geq 0 \forall k \in \mathbb{Z}_{\geq 0}$.

$$\begin{aligned}
& \mu_k \geq 0 \\
& \Rightarrow 0 < \bar{\eta}_k \leq 1 \quad (\because (4)) \\
& \Rightarrow 0 \leq \gamma_k^n \leq 1 \quad (\because \theta_k^n \leq 0, 0 < \bar{\eta}_k, 0 < c^n) \\
& \Rightarrow \gamma_k^n \|\bar{\eta}_k^n\|^2 \|\Pi_k\| + (\theta_k^n)^\top \bar{\eta}_k^n \\
& \quad = \min(1, -c^n (\theta_k^n)^\top \bar{\eta}_k^n) \|\bar{\eta}_k^n\|^2 \|\Pi_k\| + (\theta_k^n)^\top \bar{\eta}_k^n \leq 0 \\
& \quad (\because 0 < c^n < 1 / (\|\bar{\eta}_k^n\|^2 \|\Pi_k\|)) \\
& \Rightarrow c_k \leq 0 \quad (\because \text{Assumption 14}) \\
& \Rightarrow 0 \leq \gamma_k^p = \min\left(1, c^p \left(-b_k + \sqrt{b_k^2 - 4a_k c_k}\right)\right) \leq 1 \\
& \quad (\because a_k \geq 0, c_k \leq 0, 0 < c^p) \\
& \Rightarrow 0 \leq \eta_k \leq 1 \quad (\because 0 < \bar{\eta}_k \leq 1, 0 \leq \gamma_k^n \leq 1, 0 \leq \gamma_k^p \leq 1) \\
& \Rightarrow (\mu_{k+1})_i = (\mu_k)_i + \zeta \Delta t ([g(w_k)]_{\mu_k}^+)_i (\eta_k)_i \geq 0.
\end{aligned}$$

In the above, we treated that $I_k^n = \emptyset \Rightarrow \gamma_k^n = 0, \theta_k^n = 0, \bar{\eta}_k^n = 0$.

Proof of (b): It has already been proved in the above discussion.

Proof of (c): From the discussion on (a), $c_k \leq 0 \forall k \in \mathbb{Z}_{\geq 0}$. If $a_k > 0$, then

$$\begin{aligned}
0 \leq \gamma_k^p & \leq \frac{-b_k + \sqrt{b_k^2 - 4a_k c_k}}{2a_k} \quad (\because b_k \geq 0, c_k \leq 0) \\
& \Rightarrow a_k (\gamma_k^p)^2 + b_k \gamma_k^p + c_k \leq 0.
\end{aligned}$$

If $a_k = 0$, then $\gamma_k^p = 0 \Rightarrow a_k (\gamma_k^p)^2 + b_k \gamma_k^p + c_k = c_k \leq 0$. In both cases, the equalities hold if and only if $c_k = 0$.

Proof of (d): Some equal signs in Proof of (a) can be eliminated as follows.

$$\begin{aligned}
0 < \gamma_k^n & \leq 1 \quad (\because I_k^n = \emptyset, \theta_k^n < 0, 0 < \bar{\eta}_k \leq 1, 0 < c^n) \\
& \Rightarrow 0 < \eta_k^n \leq 1 \quad (\because 0 < \bar{\eta}_k \leq 1), \\
& \quad \gamma_k^n \|\bar{\eta}_k^n\|^2 \|\Pi_k\| + (\theta_k^n)^\top \bar{\eta}_k^n < 0 \quad (\because 0 < c^n < 1 / (\|\bar{\eta}_k^n\|^2 \|\Pi_k\|)) \\
& \Rightarrow c_k < 0 \quad (\because \text{Assumption 14}).
\end{aligned}$$

Proof of (e): $a_k > 0, c_k < 0 \Rightarrow 0 < \gamma_k^p = \min(1, c^p (-b_k + \sqrt{b_k^2 - 4a_k c_k})) \leq 1 \Rightarrow 0 < \gamma_k^p \leq 1$. \square

A.2 Proof of Theorem 16

PROOF. $(\Delta w_k, \Delta \mu_k, \Delta \lambda_k) = (0, 0, 0)$ yields

$$\begin{aligned}
\nabla f + \nabla g(\eta_k \circ \mu_k) + \kappa \nabla h \lambda_k & = 0, \\
\eta_k \circ [g(w_k)]_{\mu_k}^+ & = 0, \quad h(w_k; x_k) = -\alpha \lambda_k.
\end{aligned}$$

Therefore we should prove only $\eta_k \circ [g(w_k)]_{\mu_k}^+ = 0 \Rightarrow [g(w_k)]_{\mu_k}^+ = 0$. Since $\|\Pi_k\| = 0 \Rightarrow [g(w_k)]_{\mu_k}^+ = 0$, we discuss $\|\Pi_k\| \neq 0$ case below.

(i) If $I_k^n \neq \emptyset$, then $0 < \eta_k^n \leq 1, c_k < 0$ holds from Lemma 18(d). In addition, if $I_k^p \neq \emptyset$, then $a_k > 0 \Rightarrow 0 < \gamma_k^p \leq 1 \Rightarrow 0 < \eta_k^p \leq 1$ (\because Lemma 18(e)) $\Rightarrow 0 < \eta_k \leq 1 \Rightarrow [g(w_k)]_{\mu_k}^+ = 0$. If $I_k^p = \emptyset$, then $0 < \eta_k^n = \eta_k \leq 1 \Rightarrow [g(w_k)]_{\mu_k}^+ = 0$.

(ii) If $I_k^n = \emptyset$, then $c_k = c^q \lambda_{\max}(Q_{\text{all}}^d) \|z_k\|^2 \leq 0$ (\because Assumption 14), $a_k > 0$ ($\because I_k^p \neq \emptyset, \|\Pi_k\| \neq 0$). Furthermore, if $z_k \neq 0$, then $c_k < 0 \Rightarrow 0 < \eta_k = \eta_k^p \leq 1$ (\because Lemma 18(e)) $\Rightarrow [g(w_k)]_{\mu_k}^+ = 0$. If $z_k = 0$, then $\mu_k = 0$ ($\because \theta_k^p = [g(0)]_{\mu_k}^+ \circ \mu_k \geq 0, g(0) < 0$), and therefore $[g(w_k)]_{\mu_k}^+ = [g(0)]_0^+ = 0$. \square

A.3 Proof of Theorem 17

PROOF. First, we can show the following inequalities from Assumptions 7, 10 and 11.

$$\begin{aligned}
\Delta V_k^I & := w_k^\top \Delta w_k + \mu_k^\top \Delta \mu_k + \lambda_k^\top \Delta \lambda_k + \delta \zeta x_k^\top \Delta x_k \\
& \leq \zeta \Delta t \left(-\|z_k\|_{-Q_{\text{all}}}^2 + \mu_k^\top \text{diag}([g(w_k)]_{\mu_k}^+ - (\nabla g)^\top w_k) \eta_k \right), \\
\Delta V_k^{II} & := \frac{1}{2} \left(\Delta w_k^\top \Delta w_k + \Delta \mu_k^\top \Delta \mu_k + \Delta \lambda_k^\top \Delta \lambda_k + \delta \zeta \Delta x_k^\top \Delta x_k \right) \\
& \leq \zeta \Delta t \left(\|z_k\|_{Q_{\text{plant}}^d + Q_{\text{cont}}^d}^2 + \eta_k^\top \Pi_k \eta_k \right. \\
& \quad \left. + \zeta \Delta t \mu_k^\top \text{diag}((\nabla g)^\top (\nabla f + \tau \kappa \nabla h(\lambda_k + \beta h))) \eta_k \right).
\end{aligned}$$

Here, $z_k := [w_k; x_k; \lambda_k]$. Thus, the change of the function $V(w, \mu, \lambda, x) = \frac{1}{2}(w^\top w + \mu^\top \mu + \lambda^\top \lambda + \delta \zeta x^\top x)$ over discrete time steps can be evaluated as

$$\begin{aligned}
\Delta V_k & := V(w_{k+1}, \mu_{k+1}, \lambda_{k+1}, x_{k+1}) - V(w_k, \mu_k, \lambda_k, x_k) \\
& = \Delta V_k^I + \Delta V_k^{II} \\
& \leq \zeta \Delta t \left(-\|z_k\|_{-Q_{\text{all}}}^2 + \theta_k^\top \eta_k + \eta_k^\top \Pi_k \eta_k \right) \\
& \leq \zeta \Delta t \left((1 - c^q) \lambda_{\max}(Q_{\text{all}}^d) \|z_k\|^2 + a_k (\gamma_k^p)^2 + b_k \gamma_k^p + c_k \right) \\
& \leq 0.
\end{aligned}$$

Here, Assumption 14 and Lemma 18 have been used. The above discussion indicates the monotonic non-increasing property of V .

$\Delta V_k = 0 \Leftrightarrow (w_k, \mu_k, \lambda_k, x_k) = (0, 0, 0, 0)$ is shown below. Since $\Delta V_k = 0 \Leftarrow (w_k, \mu_k, \lambda_k, x_k) = (0, 0, 0, 0)$ is trivial, the following shows $\Delta V_k = 0 \Rightarrow (w_k, \mu_k, \lambda_k, x_k) = (0, 0, 0, 0)$.

Immediately from the above discussion we have $\Delta V_k = 0 \Rightarrow (w_k, \lambda_k, x_k) = (0, 0, 0)$ ($\Leftrightarrow z_k = 0$), $a_k(\gamma_k^p)^2 + b_k\gamma_k^p + c_k = 0$. From Lemma 18(c),(d), $I_k^n = \emptyset$ is necessary for $a_k(\gamma_k^p)^2 + b_k\gamma_k^p + c_k = 0$. Therefore, $\Delta V_k = 0 \Rightarrow (w_k, \mu_k, \lambda_k, x_k) = (0, 0, 0, 0)$ is confirmed as per $I_k^n = \emptyset, z_k = 0 \Rightarrow \mu_k = (\mu_k)_{I_k^p} = 0$ ($\because \theta_k^p = [g(0)]_{\mu_k}^+ \circ \mu_k \geq 0, g(0) < 0$). \square